

## Switching-time analysis of binary-oxide memristors via a nonlinear model

Nabeem Hashem<sup>a)</sup> and Shamik Das<sup>a),b)</sup>

*Nanosystems Group, The MITRE Corporation, McLean, Virginia 22102, USA*

(Received 11 October 2011; accepted 13 May 2012; published online 27 June 2012)

A simulation-based analysis is conducted of the ionic switching times for nanometer-scale binary-oxide “memristor” devices. This analysis is based upon a device model that incorporates nonlinear field-driven ionic transport within the bulk of the memristor. In contrast, prior models of charge transport in such devices have relied upon linear simplifications, or else they have included nonlinear effects only at the electrode interfaces. As shown here via simulation, the nonlinear model provides much closer quantitative agreement with experimentally observed device switching times. Also, this model predicts a distinct asymmetry between the “set” and “reset” switching behaviors of memristors that is not present in linear models. Thus, the model and the quantitative results derived using it suggest an experimental route by which the underlying device physics might be elucidated further. © 2012 American Institute of Physics.  
[<http://dx.doi.org/10.1063/1.4726421>]

In this letter, we analyze the ionic switching behavior of metal-oxide thin-film junction nanodevices using a nonlinear device model. Much attention has been focused upon recent demonstrations of hysteretic switching behavior in such devices.<sup>1,2</sup> In particular, Strukov *et al.*<sup>3</sup> recognized and Yang *et al.*<sup>4</sup> subsequently demonstrated that the current-voltage behavior of some of these devices matches that of a theoretical circuit element called a “memristor.” Device technologies and materials systems that manifest this behavior are valued for their potential to improve the density, speed, and energy efficiency of memory systems,<sup>1,5</sup> as well as other electronic systems.<sup>6–8</sup> Still, it has not yet been shown conclusively that memristor-based systems can be developed that will improve upon the write speeds of commercially available Flash memories, which are the most immediate target for industrial replacement using next-generation nanodevices.<sup>9</sup>

To a great extent this is because, until now, there has been no model that reproduces with quantitative accuracy the memristor-like behavior that has been observed in junction nanodevices. The prevalent linear models have provided only qualitative agreement with experiment.<sup>10–13</sup> For example, they reproduce the essential hysteresis and conductances, but their predicted switching times are on the order of seconds instead of being in the observed range of nanoseconds. Additionally, these linear models predict that the time to switch from a high-resistance state to a low-resistance state (i.e., the “set” time) should be equal to the time to switch in the reverse direction (i.e., the “reset” time). However, these times are observed<sup>14</sup> to be orders of magnitude different.

Here, we achieve the desired quantitative agreement with experiment by adopting a suggestion due to Strukov *et al.*<sup>15</sup> They suggested a mechanism for charge transport in binary oxides such as TiO<sub>2</sub> in which oxygen vacancies respond in a nonlinear manner to the strength of the local

electric field. Incorporating this suggestion into a linear model enables the simulated system to exhibit much shorter “set” and “reset” times. Plus, it enables the model to reproduce the observed asymmetry in these switching times.

To explain these results in detail, we begin by assuming anionic drift to be the physical mechanism underlying switching. This is believed<sup>1</sup> to be the case in binary oxides such as VO<sub>2</sub>, Ta<sub>2</sub>O<sub>5</sub>, TiO<sub>2</sub>, and other “bipolar” oxides (i.e., those that use voltages of opposite polarity for “set” and “reset” operations). In linear models of this mechanism, modulation of the device resistance is attributed to the movement via drift and diffusion of positively charged oxygen vacancies in a substoichiometric binary oxide. Specifically, the vacancy current density  $J_V(x)$  at a position  $x$  along the device is given by<sup>16</sup>

$$J_V(x) = 2q\mu EN_V(x) - 2\mu k_B T \frac{\partial N_V}{\partial x}, \quad (1)$$

where  $\mu$  is the vacancy mobility,  $E$  is the applied electric field, and  $N_V$  is the 1-D distribution of vacancies.

The key deficiency of such models is that, to match experimental data, they must assume a vacancy mobility as much as nine orders of magnitude larger than consistent with known values.<sup>11</sup> As a potential means for fixing this problem, Strukov *et al.* suggested<sup>15</sup> that vacancy drift velocity increases nonlinearly under the strong electric fields that exist in nanoscale devices. Specifically, in contrast to the usual relation  $v = \mu E$ , here the vacancy velocity  $v$  is calculated as follows:

$$v = f a \exp\left(-\frac{U_a}{k_B T}\right) \sinh\left(\frac{qE_V a}{2k_B T}\right). \quad (2)$$

In Eq. (2), the vacancy velocity is a function of the frequency  $f$  of escape attempts from the local nuclear potential wells in the device’s crystal lattice.  $U_a$  is the activation energy and  $a$  is the hopping parameter. The quantity  $E_V$  is the local electric field for an oxygen vacancy, which is related to the applied electric field by  $E_V = (1 + XF)E$ , where  $X$  is the bulk static permittivity and  $F$  is the Lorentz factor.

<sup>a)</sup>URL: <http://www.mitre.org/tech/nanotech>.

<sup>b)</sup>E-mail: [sdas@mitre.org](mailto:sdas@mitre.org).

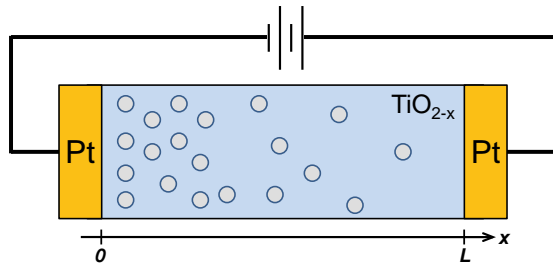


FIG. 1. Conceptual geometry for a binary oxide memristor that switches via anion migration.

The diffusion coefficient,  $D_V$ , may be calculated similarly to yield<sup>17</sup>

$$D_V = \frac{1}{2} f a^2 \exp\left(-\frac{U_a}{k_B T}\right) \cosh\left(\frac{qE_V a}{2k_B T}\right). \quad (3)$$

By combining Eqs. (2) and (3) in the same drift-diffusion treatment<sup>16</sup> used to obtain Eq. (1), we obtain a modified equation for the vacancy current density

$$J_V(x) = 2qfa \exp\left(-\frac{U_a}{k_B T}\right) \sinh\left(\frac{qE_V a}{2k_B T}\right) N_V(x) - qf a^2 \exp\left(-\frac{U_a}{k_B T}\right) \cosh\left(\frac{qE_V a}{2k_B T}\right) \frac{\partial N_V}{\partial x}. \quad (4)$$

Coupled with the continuity equation,<sup>16</sup> this modified expression determines the time evolution of the mobile vacancy distribution  $N_V(x)$  under an applied bias.

Equation (4) was employed in a finite-difference formulation to calculate quasi-steady-state electron and hole distributions and potentials for the memristor geometry given in Fig. 1. Conduction in one dimension was assumed, consistent with the formation of nanoscale-diameter conductive filaments between microscale parallel-plate contacts. These contacts at  $x=0$  and  $x=L$  were assumed to be Ohmic, with electron and hole concentrations at these boundaries determined by thermal equilibrium and space-charge neutrality. Given these initial boundary conditions, the “set” and “reset” switching characteristics of the device were investigated by applying bias potentials within the simulation and observing the elapsed simulated time.

The simulated device was started in the low-resistance state (LRS), an initial thermal-equilibrium distribution of oxygen vacancies. Positive bias was applied to the electrode at  $x=L$ , resulting in the depletion of vacancies from that side of the device. This produced a large potential barrier for electrons in the depleted region, switching the device into a high-resistance state (HRS). To set the device back into the LRS, negative bias was applied to the electrode at  $x=L$ , causing the vacancy profile to shift back toward its equilibrium distribution.

Fig. 2 provides example vacancy profiles for a 50-nm-thick device being driven from the HRS into the LRS by a  $-2\text{ V}$  applied bias. The figure shows the initial HRS profile as a solid line. Transitional profiles partway between the HRS and LRS also are shown as obtained from the nonlinear model described above (dashed red) and a linear reference

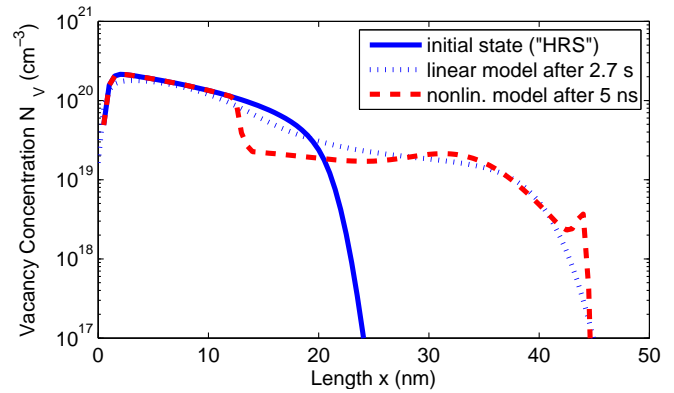


FIG. 2. Simulated profile of oxygen vacancies in a 50-nm-thick binary oxide memristor in response to an applied bias of  $-2\text{ V}$ . This memristor is configured initially in the HRS. The nonlinear model predicts a more enhanced response in regions where the vacancy concentration changes rapidly.

model (dotted blue). These profiles were chosen such that the device conductances were the same. This was done in order to contrast the predictions of the two models for the time required to reach these profiles from the HRS, as well as to illustrate the differences between the vacancy profiles predicted by the two models.

As is seen in the figure, the qualitative behavior of the vacancy profiles is consistent between the models. However, in the nonlinear model, a greater fraction of the vacancy movement occurs in the region around  $x=20$  to  $x=25\text{ nm}$ , where the HRS profile changes abruptly. Specifically, in this region, the transitional profile from the nonlinear model is seen to contain fewer vacancies than the profile for the linear model. Gradients also are seen to be sharper in the profile from the nonlinear model.

In addition, a key distinction between the two models is that the vacancy propagation occurs much more quickly in the nonlinear simulation (5 ns total switching time vs. 2.7 s using the linear model at equal bias). These switching times are calculated from the vacancy velocities using the relation  $\int dt = \int v^{-1} dx$  and summing over the finite spatial differences transited by the vacancies.

For the device modeled in Fig. 2, Fig. 3 shows switching times obtained via simulations using both the nonlinear and linear models. These were determined by analyzing the change in current as the simulated device transitioned between states. For the linear model, “set” times vary from 26 s down to 5 s under simulated device biases of 0.2 V up to 2.0 V. Using the nonlinear model, switching times decrease exponentially with increasing device voltage. In comparison to the predictions of the linear model, “set” switching times are much longer at low biases (below 1 V), yet dramatically shorter for biases exceeding 1 V. In particular, the nonlinear model predicts a “set” switching time of 44 ns at 2 V bias, consistent with the reported experimental switching time of 50 ns for a 50 nm device at a high applied bias.<sup>4</sup>

In both models, simulated “reset” switching times exhibited a much weaker dependence on the bias voltage and remained long ( $>1\text{ s}$ ) even as the voltage was set beyond 2 V. Thus, a much stronger asymmetry is seen between “set” and “reset” switching when accounting for nonlinear transport in the bulk of the device.

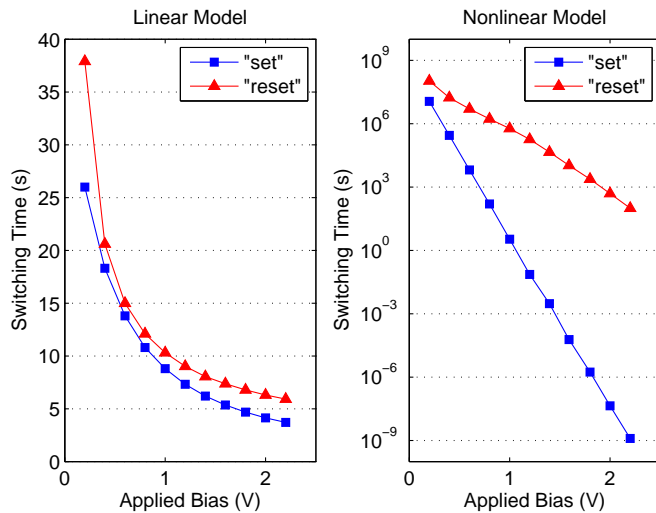


FIG. 3. Comparison between the predictions of linear and nonlinear models of memristive switching. The linear bulk model predicts a switching behavior that is largely symmetric between the “set” and “reset” switching operations. In contrast, the nonlinear bulk model predicts that the “set” operation is much faster.

The prediction of slow switching speeds in the linear bulk model is a necessary consequence of extrapolating mobility from the low-electric-field behavior of oxygen vacancies in  $\text{TiO}_2$  and similar materials. Furthermore, the linear model predicts that the “reset” switching time is nearly equal to the “set” time (the slight difference in times arises because the “set” operation works in conjunction with the natural tendency of diffusion to smooth out the vacancy concentration, whereas the “reset” operation must work against diffusion). Because ionic transport in the bulk is the dominant phenomenon underlying the switching behavior, linear bulk models necessarily must predict both slow speeds and symmetric switching times that are not observed in actual experiments on nanometer-scale  $\text{TiO}_2$  switches. More fundamentally, devices that rely upon linear electrostatic switching behavior are known to be limited by a time-voltage tradeoff,<sup>17,18</sup> in which either the switching speed or the device state retention must be insufficient for memory applications.

In contrast, the nonlinear bulk model predicts a strong asymmetry between the “set” and “reset” times. This can be explained by the strength of the internal electric field within the device during the transition between states. When the device is in the HRS, the vacancy distribution contains an abrupt, effectively vertical front that shifts toward  $x=L$  as the device switches to the LRS during a “set” operation. The resulting high electric field in the vicinity of the front promotes fast ion transport, since the ion mobility increases exponentially at high field strength. In the opposite case, when the device transitions from the LRS to the HRS during a “reset” operation, vacancies typically experience lower

fields, leading to substantially lower transport velocities and asymmetric switching behavior.

Experimental data for nanosecond-scale “set” switching times<sup>4</sup> and initial measurements of “set”-“reset” asymmetry<sup>14</sup> lend credence to the nonlinear model over linear or electrode-based approaches. However, direct quantitative comparison with experiment is hampered by a lack of exhaustive data characterizing the voltage dependence of the switching time. Also, other phenomena, such as phase transitions<sup>19</sup> or local heating,<sup>20</sup> have been proposed that could explain the initial experimental data. Nonetheless, while the 1-D electrostatic model examined here does not incorporate these phenomena or other multi-dimensional effects, it is sufficient by itself to explain the initial experimental evidence for fast switching.

Furthermore, the simulation results presented here provide a direction for more exhaustive experiments that would elucidate the physical basis of the switching asymmetry and either validate or refute the nonlinear model examined here. If validated by experiment, this model should be suitable for use in designing and optimizing resistive memory systems based upon binary-oxide memristors.

The authors gratefully acknowledge helpful comments from Dr. James Ellenbogen, Mark Taczak, and Rachel Williams of the MITRE Nanosystems Group. This research was supported by the MITRE Innovation Program and the U.S. Government Nano-Enabled Technology Initiative.

<sup>1</sup>R. Waser and M. Aono, *Nat. Mat.* **6**, 833 (2007).

<sup>2</sup>A. Sawa, *Mater. Today* **11**, 28 (2008).

<sup>3</sup>D. B. Strukov, G. S. Snider, D. R. Stewart, and R. S. Williams, *Nature (London)* **453**, 80 (2008).

<sup>4</sup>J. J. Yang, M. D. Pickett, X. Li, D. A. A. Ohlberg, D. R. Stewart, and R. S. Williams, *Nat. Nano* **3**, 429 (2008).

<sup>5</sup>K. Galatsis, K. Wang, Y. Botros, Y. Yang, Y.-H. Xie, J. F. Stoddart, R. B. Kaner, C. Ozkan, J. Liu, M. Ozkan, C. Zhou, and K. W. Kim, *IEEE Circuits Devices Mag.* **22**, 12 (2006).

<sup>6</sup>G. S. Snider and R. S. Williams, *Nanotechnology* **18**, 035204 (2007).

<sup>7</sup>K. K. Likharev, *J. Nanoelectron. Optoelectron.* **3**, 203 (2008).

<sup>8</sup>A. C. Cabe and S. Das, *Nanotechnology* **20**, 165203 (2009).

<sup>9</sup>Semiconductor Industry Association, *International Technology Roadmap for Semiconductors: 2011 Edition*, Washington, DC.

<sup>10</sup>D. B. Strukov, J. L. Borghetti, and R. S. Williams, *Small* **5**, 1058 (2009).

<sup>11</sup>D. S. Jeong, H. Schroeder, and R. Waser, *Phys. Rev. B* **79**, 195317 (2009).

<sup>12</sup>Z. Biolk, D. Biolk, and V. Biolková, *Radioengineering* **18**, 210 (2009).

<sup>13</sup>Y. N. Joglekar and S. J. Wolf, *Eur. J. Phys.* **30**, 661 (2009).

<sup>14</sup>Y. H. Do, J. S. Kwak, Y. C. Bae, K. Jung, H. Im, and J. P. Hong, *Appl. Phys. Lett.* **95**, 093507 (2009).

<sup>15</sup>D. B. Strukov and R. S. Williams, *Appl. Phys. A* **94**, 515 (2009).

<sup>16</sup>Y. Taur and T. H. Ning, *Fundamentals of Modern VLSI Devices*, 2nd ed. (Cambridge University, Cambridge, UK, 2009).

<sup>17</sup>M. Noman, W. Jiang, P. A. Salvador, M. Skowronski, and J. A. Bain, *Appl. Phys. A* **102**, 877 (2011).

<sup>18</sup>H. Schroeder, V. V. Zhimov, R. K. Cavin, and R. Waser, *J. Appl. Phys.* **107**, 054517 (2010).

<sup>19</sup>T. Chang, S.-H. Jo, K.-H. Kim, P. Sheridan, S. Gaba, and W. Lu, *Appl. Phys. A* **102**, 857 (2011).

<sup>20</sup>S. Menzel, M. Waters, A. Marchewka, U. Böttger, R. Dittman, and R. Waser, *Adv. Funct. Mater.* **21**, 4487 (2011).